Energy 299 (2024) 131435

Contents lists available at ScienceDirect

Energy

journal homepage: www.elsevier.com/locate/energy

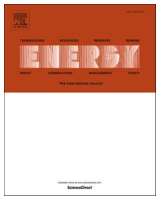

Enhancing thermal conductivity of sinterized bronze (Cu89/Sn11) by 3D printing and thermal post-treatment: Energy efficiency and environmental sustainability

Rubén Lostado-Lorza *, Marina Corral-Bobadilla, Celia Sabando-Fraile, Fátima Somovilla-Gómez

Industrial Engineering, Department of Mechanical Engineering University of La Rioja, C/José de Calasanz 31, 26004, Logroño, La Rioja, Spain

ARTICLE INFO

Handling Editor: Dr. Henrik Lund

Keywords:
Thermal conductivity
Life cycle assessment
Fused deposition modeling (FDM)
Sustainability in manufacturing
Environmental impact

ABSTRACT

Enhancing the thermal conductivity of bronze is essential to enhance the efficiency of heat transfer and reduce energy consumption in systems such as heating, cooling, and heat exchangers systems. This study investigates the feasibility of producing sinterized bronze (Cu89/Sn11) using low-cost 3D printing Fused Deposition Modeling (FDM) technology and thermal post-treatment processes. The intention is to identify optimal printing parameters and sintering temperatures to maximize thermal conductivity, while focusing on minimizing energy consumption, raw material usage, and environmental impact. The thermal conductivity of twenty-seven samples was evaluated according to the ASTM E1530:2019 standard. A statistical analysis revealed significant effects of nozzle diameter and flow rate on thermal conductivity and density. The optimal results were obtained with a sintering temperature of 845 °C, a 1.0 mm nozzle diameter, and a 110 % flow rate. These conditions yield the highest thermal conductivity (87.61 W/m·K) and density (7.52 g/cm^3). The lowest values were observed at a sintering temperature of 865 °C, a 0.6 mm nozzle diameter, and a 100 % flow rate. A Life Cycle Assessment (LCA) using the ReCiPe Endpoint (E) methodology was employed to compare the environmental impact of the resulting thermal conductivities. The results suggest that sintered bronze produced by FDM and thermal post-treatment provide superior performance and a smaller environmental impact than conventional methods. This study underscores the potential for more efficient and sustainable manufacturing practices in the production of sintered bronze.

1. Introduction

High thermal conductivity of bronze facilitates efficient transfer of heat transfer reduces energy loss in heating, cooling, and heat exchanger systems. Its resistance to corrosion, durability and compatibility with thermal fluids positions it as a sustainable and efficient material. Currently, a wide range of components used in heating, cooling, and heat exchanger installations, such as valves, heat exchangers, pipes, connections, ducts, valves, pumps, temperature sensors and boiler accessories, are manufactured with this material [1]. Most of these components are manufactured by conventional processes, such as casting and machining, which require considerable amounts of energy and raw materials [2]. These manufacturing processes may have limitations when the shapes of the components to manufacture are more complex. In contrast, 3D printing has gained considerable attention by allowing the creation of components with complex geometries, in a shorter production time, thus generating little material waste and reducing energy consumption [3]. In recent years, polymers, such as Polylactic Acid (PLA), is blended with metallic micro powders (mainly steel, aluminum, copper and bronze), and arranged in the form of filaments. This allows the manufacture of 3D objects of complex s0hapes by low-cost 3D printers based on Fused Deposition Modeling (FDM) technology. This strategy shows promise in manufacturing components with complex shapes, and high thermal conductivity by using large concentrations of thermally conductive metal particles, while reducing energy and raw material consumption. These printable metal-polymers often undergo a multi-stage sintering process after 3D printing that involves subjecting them to high temperatures and regulated atmospheres at high pressures

* Corresponding author.
E-mail addresses: ruben.lostado@unirioja.es (R. Lostado-Lorza), marina.corral@unirioja.es (M. Corral-Bobadilla), celia.sabando@unirioja.es (C. Sabando-Fraile), fatima.somovilla@unirioja.es (F. Somovilla-Gómez).

https://doi.org/10.1016/j.energy.2024.131435
Received 13 February 2024; Received in revised form 25 March 2024; Accepted 24 April 2024
Available online 5 May 2024

for extended periods of time [4]. Sintering increases the density, thermal conductivity and mechanical strength of the printed material by increasing the number of thermal contacts between metallic particles. This occurs when the PLA binder is removed [5]. There are several studies that have examined the thermal properties of unsintered printable metal-polymers by FDM 3D technology [6]. The results of these investigations show that the thermal conductivity values obtained are reduced in comparison to those of the pure metal itself. However, the thermal properties of sintered printable metal-polymers and methods for improving them have been the subject of relatively few studies. Thus for example, Ebrahimi and Ju [7] conducted an experimental study to assess the thermal of samples that were printed with filaments that were made of polymer-copper composites with a copper powder fraction between 87.0 % and 90.7 %. In this case, a first debinding stage was conducted at 350 °C for 3 h, whereas the sintering process was carried out at 980 °C for 50 min. Finally, an over-sintering process is carried out at a temperature of 1080 °C for 10 min on some samples. The results for the samples manufactured by FDM 3D printing were compared to those for samples manufactured by model with pressures of 200 kPa. The results showed that the printed samples that were subjected to the debinding and sintering processes presented thermal conductivity values of approximately 30 W/m·K, whereas those that were subjected to over-sintering at 1080 °C presented values of the order of 60 W/m·K and an excessive deformation of the samples. Other authors, such as Cañadilla et al. [8], determined the thermal conductivity of samples manufactured by FDM based on a polymer-copper composite printable filament with a copper powder fraction of over 95 wt%. An initial debinding process was conducted. It consisted of the partial elimination of the paraffin present in the PLA by immersing the printed samples in a chemical solvent. Next, a thermal debinding followed by high temperature sintering was undertaken. Both thermal processes were carried out in an furnace with a protective atmosphere that included a mixture of 2.8 % H_2-97.8%Ar for the total duration of the thermal process of about 30 h. The conductivity values obtained in this case were 363 ± 9 W/m·K. However, more recently Lostado et al. (2023) [9] conducted a preliminary investigation to determine the tensile strength, elastic modulus and thermal conductivity of samples manufactured with PLA-bronze (Cu89/Sn11) using FDM 3D printing technology. In that work, the average thermal conductivity results obtained for this material were 82.68 W/m·K with a sintering temperature of 858 °C and a nozzle diameter of 0.6 mm. However, to date no further references have been found in which the thermal conductivity and methods for improving it for the PLA-bronze (Cu89/Sn11), despite it being an easily printable and sinterable material.

Life Cycle Assessment (LCA) is a methodological tool that is used to evaluate the environmental impacts of a product, service or process during its entire life cycle, from the extraction of raw materials to its final disposal. The primary aim of Life Cycle Assessment (LCA) is to comprehend and measure the environmental impacts at every stage of the life cycle of a product. This understanding enables informed decision-making to enhance its environmental performance. Even though FDM technology is thought to be a clean production method, there are specific health hazards that are associated with 3D printing PLA components. Prolonged exposure to certain compounds during this process can have adverse effects on human health. Some studies have quantified emission rates of various VOCs during 3D printing for different filaments [10]. However, most LCA studies of metal powder sintering processes have largely examined the use of energy, water, materials, natural resources, and transportation to the plant (cradle--to-grave) [11]. As in the case of FDM, some LCA investigations of casting processes have concerned only on the use of raw materials, water, and energy at a laboratory scale (gate-to-gate) [12]. Other LCA investigations of casting processes have expanded their scope (cradle to the grave) to involvement in the environmental inventory (1) the assessment of energy, water, materials, and natural resources, (2) the emissions to air, water, and soil, and (3) the transport stage [13]. Studies generally agree that FDM offers environmental advantages over conventional manufacturing methods like casting and machining, although the extent of these benefits varies by industry [14]. However, the extent of these benefits depends on the specific industry in which FDM is used [15]. Also, the small amount of wasted material and lower energy use are two key environmental benefits of powder metallurgy and the sintering processes [16]. Although many LCA studies have concentrated on traditional manufacturing processes like machining and casting, few have evaluated FDM [17]. The majority of LCA studies of FDM have focused on material and energy consumption on a laboratory scale [18]. Also, to date no reference has been found in which an in-depth LCA of an FDM manufacturing process followed by a sintering process has been conducted.

The current work investigates the feasibility of producing sintered bronze (Cu89/Sn11) using low-cost 3D printing Fused Deposition Modeling (FDM) technology, along with debinding and sintering thermal post-treatment processes in a conventional furnace without a controlled atmosphere. The main goal is to identify optimal printing parameters (nozzle diameter and flow rate) and sintering temperature to achieve the highest thermal conductivity values for sinterized bronze Cu89/Sn11, while emphasizing the reduction of energy consumption, raw material usage, and environmental impact in the production process. The thermal conductivity of this material is determined according to the ASTM E1530:2019 standard [19]. An exhaustive life cycle analysis (LCA) is conducted employing the ReCiPe Endpoint (E) impact methodology to determine the environmental impact of the complete manufacturing processes for the samples that have the highest and lowest thermal conductivity. The resulting thermal conductivity and environmental impact results were compared to those of the same material that were produced by casting and subsequent machining. Finally, in order to determine the reason for the notable variation in thermal conductivity of sinterized samples, an analysis of the microstructure and chemical composition was undertaken by Scanning Electron Microscope (SEM) and Energy Dispersive X-ray (EDS).

2. Experimental section

2.1. Selection of materials and printing parameters

All samples for thermal conductivity measurement were manufactured by using 3D printing filaments of PLA-bronze that was supplied by filament2print [20] and manufactured by the virtual foundry [21]. Table 1 summarizes the most significant characteristics of this filament.

This commercial filament can be printed by conventional 3D printer machines with FDM technology and also requires no furnaces with controlled atmospheres for the debinding and sintering processes. The printed samples are known as the “green part.” Because of its non-homogeneous composition, it lacks substantial mechanical integrity [22]. In this work, all samples were printed by a commercial 3D printer machine Duplicator 6 produced by Wanhao Co., China. Hardened material nozzles with different diameters and capable of resisting wear and abrasion at high temperatures were provided by Micro-Swiss Co., Ltd USA. The production of parts using FDM technology is widely acknowledged to be influenced by several printing parameters, with the most important being fill pattern, fill density, extrusion temperature, bed temperature, print speed, layer height, nozzle diameter, material flow and part orientation. In this research, nozzle diameter and flow rate

Table 1
PLA-bronze filament characteristics.

Filament Diameter (mm)	*Metal/PLA (%)*	*Cu/Sn* (%)	Melting Temperature (°C)	Themal Decomposition (°C)	Metal Particles Diameter (mm)
1.75	*87*	*89*	*140–170*	*240*	*10*-50 μm

percentage parameters were considered as study variables in order to determine their effect on thermal conductivity. Commercial nozzle sizes of 0.6, 0.8, and 1 mm, and flow rate percentages of 100 %, 105 %, and 110 %, were considered in this research. The diameter of the nozzle in 3D printing directly affects the amount of printing material deposited. Larger nozzle diameters allow a greater amount of deposited material on each layer, whereas a smaller nozzle restricts the amount of material that can be deposited. Similarly, flow rate percentage determines (in %) the amount of filament that flows through the nozzle during the printing process. It is well known that the combination of the parameters mentioned can significantly affect the porosity of the printed (green samples) and sinterized samples and, therefore, their thermal conductivity [8]. For example, Fig. 1 shows the pores that were generated between the gap in the deposited material when different green samples are printed by using 1.0 mm nozzles and maintaining the layer height as constant. Two different flow rates are shown (100 % and 110 %). Fig. 1a presents a micrograph including a cross-sectional view and a top view of the outer layer of the printed green sample when considering a flow rate of 100 %. Similarly, Fig. 1b shows a micrograph including a cross-sectional view and a top view when considering a flow rate of 110 %. When examining both figures, it can be seen that the pore size that was generated is significantly larger when printing the green sample at a flow rate of 100 %, than when printing the same sample at a flow rate of 110 %.

Finally, for all samples that were studied, two lines were considered for the wall thickness [23]. The filling pattern considered was linear, with a raster angle of −45° and 45° [24]. The remaining printing parameters, such as layer height, shell thickness, hot end temperature, bed temperature, flow rate, fill density and print speed, were considered as fixed parameters, and are summarizes in Table 2.

Table 2
3D printing parameters.

3D Printing parameters	Minimum	Intermediate	Maximum
Nozzle Diameter (mm)	0.6	0.8	1
Flow Rate (%)	100	105	110
Layer Height (mm)=0.5 Nozzle Dimeter*	0.3	0.4	0.5
Shell Thickness (mm)	0.4	0.4	0.4
Hot End Temperature (°C)	220	220	220
Bed Temperature (°C)	50	50	50
Infill Density (%)	100	100	100
Print Speed (mm/S)	35	35	35

2.2. Selection of debinding and sintering temperatures

In the current work, the thermal post-treatment based on debinding and sintering processes for all samples were conducted in a conventional muffle furnace HK-11 from Hobersal Co., Ltd Spain. These thermal processes were applied successfully to FDM 3D printing technology for the first time in 1996 [25]. During the debinding process, most of the binders and the PLA that were present in the "green samples" were eliminated, giving rise to what is known as "brown samples." Brown samples are extremely fragile as there is very little polimeric material left to join them. Green samples must be free of defects, such as bubbles or impurities, in the polymer. These could create points of instability during the debinding and sintering processes. It is very important that during the debinding process, brown samples should not begin to flow under gravitational load to avoid excessive deformations in the sintered samples. Finally, the sintering process facilitates the cohesion and compaction of the metallic powder particles, resulting in the formation of the final component [26]. In recent years, different procedures to carry out the debinding process have been proposed. Among them, the processes that require a controlled atmosphere those with pressure and temperature [7], those with temperature and chemical solvent [8] and those with a catalyst such as gaseous nitric acid (HNO_3) [27]. In the current research, preliminary experiments of debinding and sintering processes were conducted according to the suggestions of the PLA-bronze filament manufacturer. The debinding process was undertaken at 465 °C for 4.5 h, reaching this temperature in 1 h. At the end of this phase, a layer of activated carbon weighing 150 g was added. The incineration of this activated carbon in the furnace protected the brown samples from oxidation during the sintering process, by raising the concentration of carbon dioxide and reducing that of oxygen [28]. The sintering temperature was considered as a temperature to study in the current paper, as it could significantly affect the thermal conductivity. In this case, three different sintering temperatures, namely 845 °C, 855 °C and 865 °C, and a duration of 3 h for each were proposed. As mentioned above, the sintering temperature is very important. It can affect the

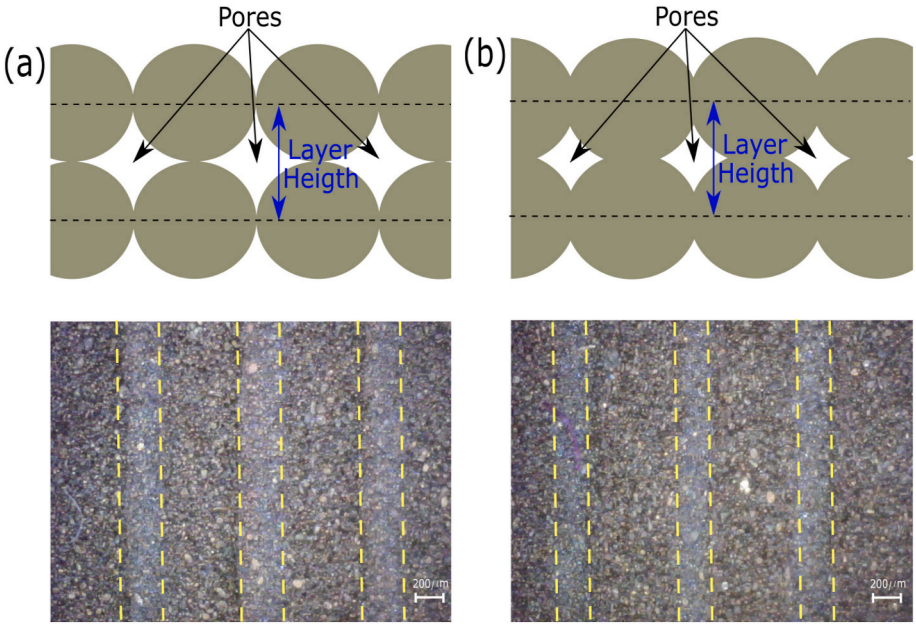

Fig. 1. Pores generated between the deposited material when different green samples are printed using 1.0 mm nozzles, and maintaining the layer height as constant (images at a magnification of 50×): (a) flow rate of 100 %. (b) flow rate of 110 %. (For interpretation of the references to colour in this figure legend, the reader is referred to the Web version of this article.)

increase in thermal contact between the metal particles and, consequently, the increase in thermal conductivity. However, excessive values of sintering temperature can cause excessive deformations of the sintered samples. Fig. 2 shows the thermal post-treatment curves which indicate the suggested temperatures for debinding and sintering to bed studied, together with the corresponding residence period and heating rate, the point of the addition of activated carbon and the state that each sample reaches (green, brown and sinterized).

2.3. Design of Experiments (DoE)

A Design of Experiments (DoE) is a statistical methodology that is used to determine the minimum number of experiments required to support a stated hypothesis. This ensures that the entire range of possibilities is covered in a homogeneous manner, and also that the experiments to be conducted are representative [29]. Various methodologies exist for developing a Design of Experiments (DoE). All require the creation of a design matrix that incorporates input variable or input parameters and output variables [30]. In this case, a 3^K Full Factorial Design that considers three levels and three inputs was chosen ($K = 3$). Based on the DoE selected, 27 experiments are required to determine the influence of the input parameters or independent variables (Nozzle Diameter (mm), Flow Rate (%), and Sintering Temperature (°C)) on the output or dependent variables (Thermal conductivity). Table 3 summarizes the input parameters, the range and the levels needed to implement the DoE based on 3^K Full Factorial Design. Once the factors and levels have been set as in this table, the design matrix and their corresponding combination of input parameters (See Table 4) are generated by the "R'' statistical software [31].

2.4. 3D printing of the green samples

It is well known that after the debinding and sintering processes, the printable metal-polymer green samples that were manufactured by FDM suffer enormous thermal shrinkage. This is due mainly to evaporation of the polymer, which is very difficult to predict in advance. This thermal shrinkage depends largely on the main printing direction on each of the axes (X, Y and Z), the printing pattern used, the size and quantity of the pores that are generated, the nozzle diameter, as well as the debinding and sintering temperatures [8]. In order to achieve the goal of obtaining

Table 3
Experimental design levels and independent variables used with the proposed 3^K Full Factorial DoE.

Input parameters	Minimum	Intermediate	Maximum
Nozzle Diameter (mm)	0.6	0.8	1
Flow Rate (%)	100	105	110
Sintering Temperature (°C)	845	855	865

already sintered samples with precise dimensions on each of the X, Y, and Z axes in accordance with the ASTM E1530:2019 [19], and thus determine the thermal conductivity of the sintered PLA-bronze, the following steps were proposed. They were proposed with the intention of taking into account the volume reduction percentages that are associated with the 27 printing parameters and sintering temperatures that appear in Table 4. First, 27 hexahedrons (or green samples) with dimensions of 20 mm × 20 mm x 20 mm were printed and then sintered in the 3D printer machine Duplicator 6 and in the HK-11 muffle furnace respectively, according to their corresponding printing parameters and sintering temperatures that are shown in Table 4. After all hexahedrons samples were sintered, their percentage of mass and shrinkage on each of the X, Y and Z axes were determined. Table 6 sumarizes these reduction percentages obtained for of each of the 27 green samples. To compensate for the volume reduction, each shrinkage on each of the X, Y and Z axes were considered for modelling the green samples according to ASTM E1530:2019. In this case, a DTC-25 thermal conductivity meter produced by TA Instruments Co., Ltd USA was used to measure the thermal conductivity of the sintered PLA-bronze samples. This indicateds that, the already sintered specimens (i.e., those that had undergone thermal shrinkage on each of the X, Y and Z axes) must be cylinders with a diameter of 50 mm and a height of at least 1.25 mm. In this study, after conducting various preliminary tests to determine correctly the thermal conductivity, it had been shown that the most appropriate dimensions for the specimens are 50 mm in diameter and 5.5 mm in height. Table 8 shows the dimensions prior to the sintering process (greeen samples), the percentages of mass and volume reduction, as well as each of the final dimensions of each of the 27 cylinders after their sintering process. All 3D-printed green samples (i.e., the 27 hexahedrons of dimensions 20 mm × 20 mm x 20 mm, as well as the 27 cylinders considering their percentage reduction) were modeled by

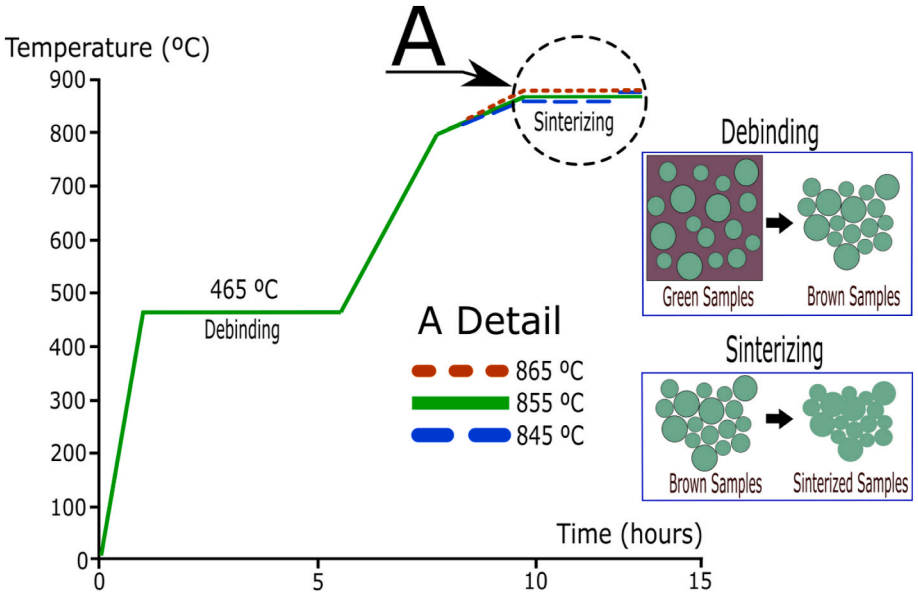

Fig. 2. Thermal post-treatment curves: temperatures, residence periods and heating rates for debinding and sintering; the addition of activated carbon and the state the samples reach (green, brown and sinterized). (For interpretation of the references to colour in this figure legend, the reader is referred to the Web version of this article.)

Table 4
Design matrix and experiments obtained by 3^K.

Sample	Nozzle Diam. (mm)	Flow Rate (%)	Sintering Temp. (°C)	Sample	Nozzle Diam. (mm)	Flow Rate (%)	Sintering Temp. (°C)
01	*0.6*	*110*	*845*	*15*	*0.6*	*100*	*865*
02	*0.6*	*100*	*855*	*16*	*1.0*	*110*	*855*
03	*0.8*	*105*	*865*	*17*	*1.0*	*105*	*855*
04	*0.6*	*105*	*865*	*18*	*0.6*	*100*	*845*
05	*0.8*	*110*	*845*	*19*	*0.6*	*110*	*865*
06	*1.0*	*110*	*845*	*20*	*0.8*	*100*	*865*
07	*1.0*	*100*	*865*	*21*	*1.0*	*105*	*865*
08	*1.0*	*110*	*865*	*22*	*0.8*	*100*	*855*
09	*1.0*	*100*	*845*	*23*	*0.8*	*110*	*865*
10	*0.8*	*105*	*845*	*24*	*0.8*	*105*	*855*
11	*0.8*	*100*	*845*	*25*	*1.0*	*105*	*845*
12	*0.6*	*110*	*855*	*26*	*0.6*	*105*	*855*
13	*0.6*	*105*	*845*	*27*	*1.0*	*100*	*855*
14	*0.8*	*110*	*855*	-	-	-	-

SolidWorks® 2022 CAD software [32]. Then, the 3D models were sliced using the Ultimaker Cura 5.0.0 software [33] in order to create the G-codes necessary for printing the green samples on the 3D printer. The electrical power required for FDM 3D printing of the 27 metal-polymer green samples was measured by a D52-2047 power meter that was produced by KetoteK Co., Ltd China. This power had been ussed to determine the environmental impact using Life Cycle Assessment (LCA). Fig. 3 shows some examples of volume reduction that was produced by thermal shrinkage after siterization. Fig. 3a shows the volume reduction that green hexahedron samples experience during sintering when the initial dimensions are 20 mm × 20 mm x 20 mm. Fig. 3b shows the volume reduction caused by sintering the green cylinders that, after their sintering process, its required dimensions are 50 mm in diameter and 5.5 mm in height according to ASTM E1530:2019. Fig. 3c shows one of the sintered cylinders mounted on the DTC-25 thermal conductivity meter in order to determine its thermal conductivity.

2.5. The thermal post-treatment

As mentioned previously, the thermal post-treatment of debinding and sintering was conducted in a conventional muffle furnace HK-11 with the temperature controlled. To ensure the precision and comparability of all reduction percentages and conductivity values that were obtained subsequent to thermal post-treatment, the steps that followed were meticulously developed. Due to the absence of a protective atmosphere in the furnace used for this investigation and following manufacturer recommendations, all sintered green samples were heated in a 316L stainless steel crucible, and covered completely by an alumina powder coating. This coating, which had a total thickness of 40 mm, prevented direct contact with oxygen in the air and ensured that the temperature surrounding the green samples was uniform. The alumina powder, when compacted, is responsible for maintaining the geometry of the piece and preventing it from suffering deformation. Furthermore,

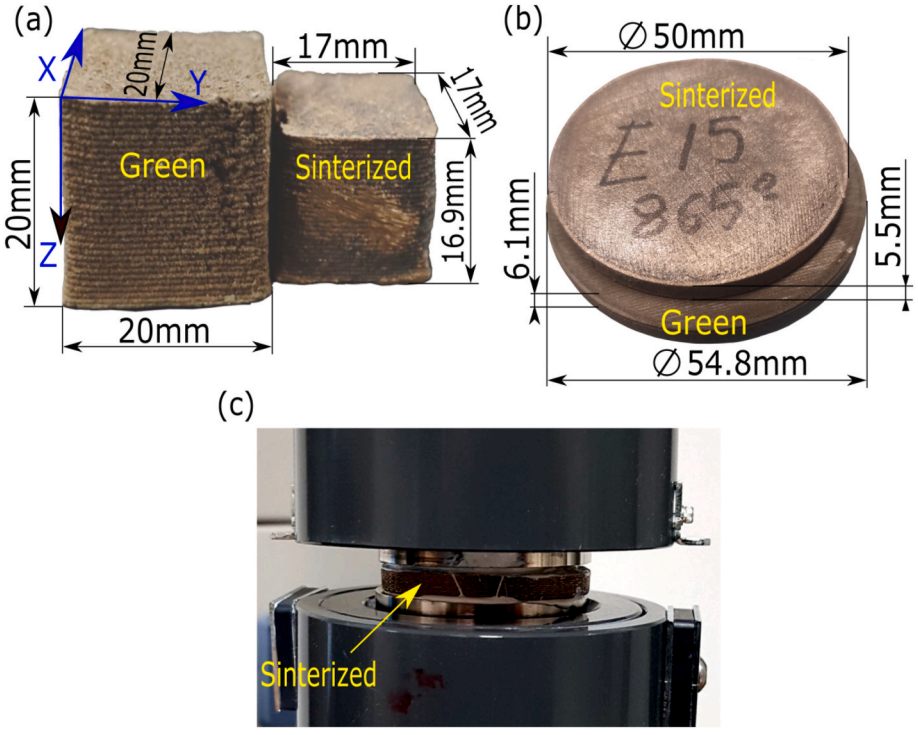

Fig. 3. (a) Volume reduction produced by the thermal shrinkage after sintering the green hexahedrons with initial dimensions of 20 mm × 20 mm x 20 mm. (b) Volume reduction produced by the thermal shrinkage after sintering the green cylinders according to the ASTM E1530:2019 test with required dimensions of 50 mm in diameter and 5.5 mm in height. (c) Details of the cylindrical sample mounted on DTC-25 thermal conductivity meter in order to determine its thermal conductivity. (For interpretation of the references to colour in this figure legend, the reader is referred to the Web version of this article.)

as it is a porous medium, it favors the evacuation of gases generated during the incineration of PLA during the debindingand sintering process. After the thermal post-treatment of debinding was completed at a temperature of 465 °C, a 30 mm layter of activated carbon (150 g) was added on top of the alumina powder coating. As mentioned previously, the purpossse of this activated carbon layer was to prevent the samples from being completely oxidized during the sintering process. The recommendations provided by the filament manufacturer regarding the spacing between samples and also between the samples and the walls of the 316L stainless steel crucible were followed. As a result, it was decided to sinter three hexahedral specimens together in a single thermal post-treatment to determine the volume reduction, as well as to sinter one cylindrical specimen separately for thermal conductivity testing. To reduce experimental discrepancies and assure repeatability, the samples were processed in triplicate. Fig. 4 shows the procedure that was followed for the thermal post-treatment of debinding and sintering processes of all the samples that were studied. Fig. 4a shows a cylindrical specimen that used an insufficient amount of activated carbon. It can be seen in the figure that this sample has been oxidized completely. Fig. 4b shows the interior of the crucible, which contains a layer of alumina powder approximately 20 mm deep and with the green sample 01 on top of the layer of alumina powder. Fig. 4c details elements required to correctly carry out the sintering of a sample and avoid its oxidation. The electrical power required for the thermal post-treatment of debinding and sintering was also measured by a D52-2047 power meter. This power required and the activated carbon used were then utilized to assess the environmental impact using Life Cycle Assessment (LCA).

2.6. Manufacturing by gravity casting and machining

A sample of bronze Cu89/Sn11 (sample 28) was manufactured by gravity casting and machining in accordance with the specifications outlined in the ASTM E1530:2019. The objective was to determine its thermal conductivity, its density, and its environmental impact generated during both processes. In this way, the thermal conductivity that would be obtained would not be affected by the printing parameters if these processes were used, and the sample could be completely free of defects and pores. The results were compared to those results obtained from the 27 samples manufactured by FDM and its subsequent debinding and sintering processes. The steps involved in manufacturing the sample 28 including gravity casting and machining, are illustrated in Fig. 5. Firstly, remains of bronze Cu89/Sn11 from preliminary tests are fused in a graphite crucible utilizing the conventional muffle furnace HK-11 that was employed for the debinding and sintering processes (Fig. 5a). The remains of bronze used in this case had a mass of 145 g which was sufficient to produce a sample with dimensions of 50 mm in diameter and 5.5 mm in height after the machining process. To prevent oxidation of the bronze at high temperatures and facilitate its fusion, sodium tetraborate (commonly known as borax) was added inside of the crucible when the temperature reached within the furnace was 980 °C (Fig. 5b). The remaining bronze endured a complete fusion process within 4 h, of which three were required to attain a temperature of 1000 °C. That temperature was maintained for an additional hour to (Fig. 5c). Following the fusing of the bronze remnants, and after the temperature had dropped to room temperature, a solid bronze cylinder was taken from the crucible and machined until it measured 50 mm in diameter and 5.5 mm in height according to ASTM E1530:2019 (Fig. 5d). After sample 28 was machined, its mass, density and thermal conductivity were determined. In the same way that the electrical power required for the manufacture of the 27 samples was measured, the electrical power required throughout the bronze fusion process and its final machining was also measured using a D52-2047 power meter produced by KetoteK Co., Ltd China. The electrical power consumed, the mass of bronze shavings produced, and the amount of sodium tetraborate required were subsequently incorporated into the Life Cycle Assessment (LCA) to evaluate the environmental impact of manufacturing by gravity casting and machining the sample of bronze Cu89/Sn11.

2.7. Life cycle assessment (LCA)

A widely recognized approach of methodically evaluating the environmental effect of processes, goods, and activities is Life Cycle Assessment (LCA). It was developed in the 1990s based on the ISO

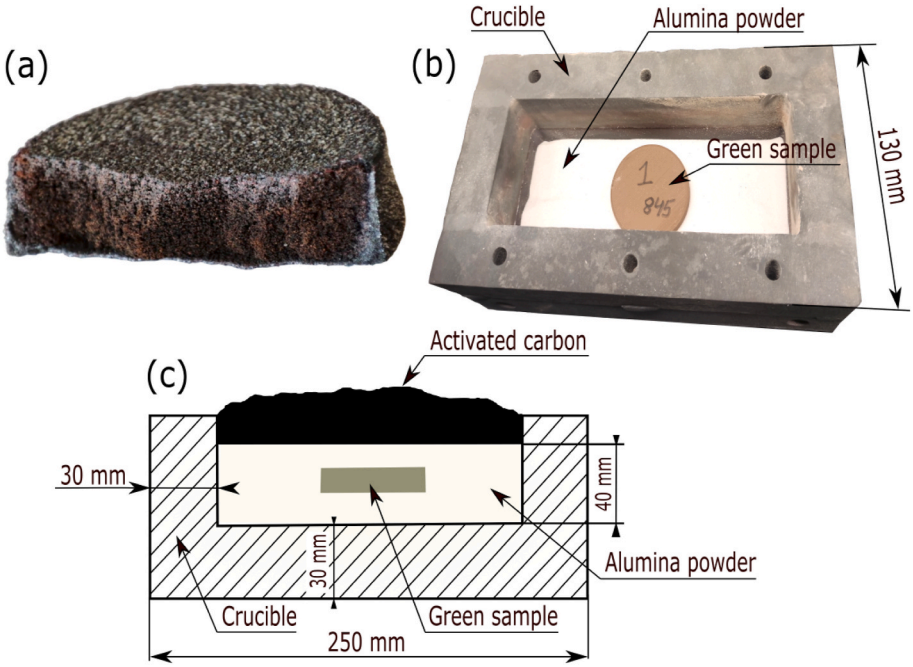

Fig. 4. (a) Cylindrical sample that has undergone complete oxidation due to an insufficient amount of activated carbon used. (b) Layer of alumina powder with green sample 1 on top of this layer. (c) Elements required for correct sintering of a sample and thus avoiding its oxidation. (For interpretation of the references to colour in this figure legend, the reader is referred to the Web version of this article.)

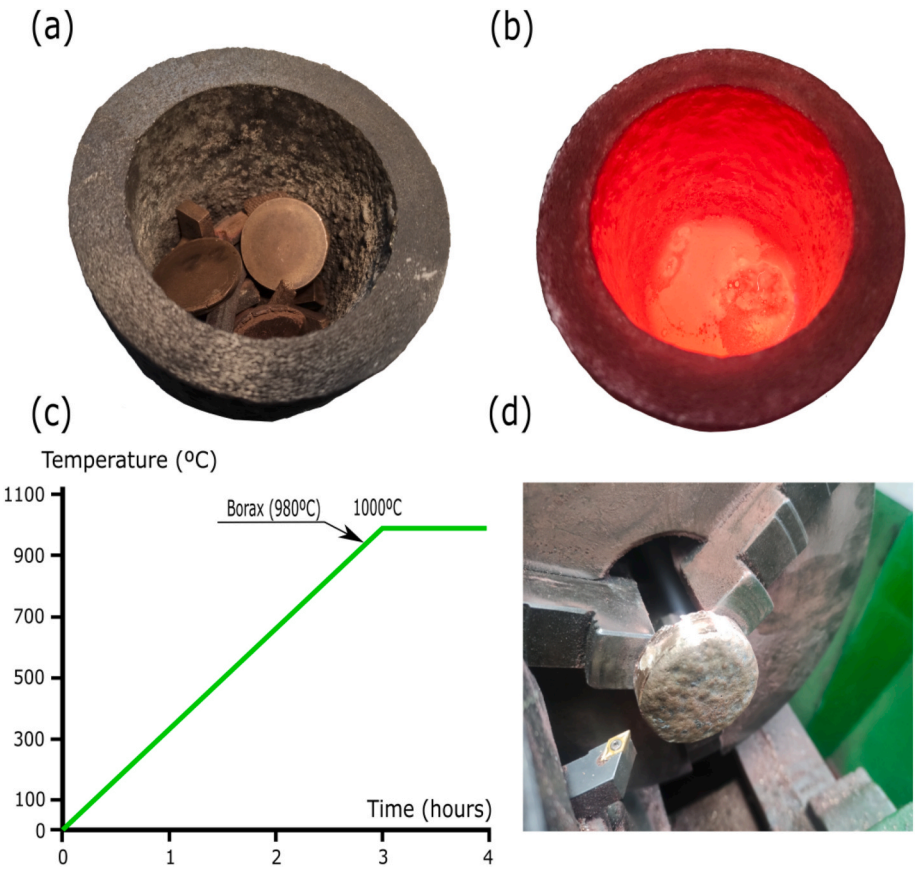

Fig. 5. Steps involved in producing the sample 28 according to ASTM E1530:2019 from remains of bronze Cu89/Sn11: (a) Bronze remains that were collected for fusing in a graphite crucible. (b) Addition of sodium tetraborate to the molten remains of bronze when its temperature is 980 °C. (c) The temperatures and times required to achieve the full fusion of the remains of bronze. (d) Machining process of the sample in accordance with the ASTM E1530:2019, with the dimensions of 50 mm in diameter and 5.5 mm in height.

14040 [34] and 14,044 [35] standards. Given the intricacy of the calculations and algorithms necessary for accurate LCA, software is often used to facilitate the environmental assessment [36]. The SimaPro software has gained extensive use over the years in conducting LCA studies due to its many benefits. These include its exceptional adaptability, user-friendly interface, and the ability to integrate other databases, such as Ecoinvent [37]. The stages of LCA are outlined in ISO 14040 and include four key steps. Firstly, there is the identification and characterization of the specific case, product, or process to be assessed. Secondly, data is gathered on the environmental burdens that are associated with the identified case. Thirdly, the effect of these burdens on the environment is quantitatively evaluated by an impact assessment. Lastly, the results obtained from the LCA are interpreted. The LCA outcomes are measurable, enabling researchers to compare newer manufacturing methodologies with older ones or with presently competing alternatives, such as casting or machining [18]. There are different methodologies to perform an LCA. They are Eco-Indicator, ReCiPe and CML. However, to date, ReCiPe is the most commonly used methodology in LCA for manufacturing components using FDM [38].

Despite being considered to be a clean manufacturing technique, the 3D printing of components in PLA with FDM technology involves some risks to human health. These include emissions of particulate aerosol of sizes between 7.8 and 10.5 nm [39], as well as volatile organic compounds (VOCs) including methylmethacrylate [40]. In addition, the debinding and sintering processes involve a complete incineration of the PLA. This produces an increase in CO_2 emissions of 673 g–4605 g per kilogram of PLA burnt [41]. The activated carbon that is used to prevent the oxidation of the samples during the sintering process produces NOx, CO, CO_2 and CH_4 when it is incinerated [42]. Different methodologies, such as ReCiPe (endpoint and midway), EPS, Ecoindicator, and CML, have been used to perform an LCA in machining processes. Among these methodologies, ReCiPe endpoint is the one that is most commonly employed for a study at laboratory scale (gate-to-gate), followed by CML [43]. Energy and water consumption, along with waste generation, cooling fluids, lubrication, and chips removal, have been considered consistently in life cycle assessment (LCA) studies for machining processes [44]. However, energy consumption during machining is considered in most LCA studies as one of the greatest generators of environmental impacts [18]. In this research, the LCA was undertaken using the ReCiPe Endpoint (E) impact methodology. This was implemented in Ecoinvent 3, which was integrated into the Simapro® v.9.2.0.2. software. This methodology quantifies Human health, Ecosystems and Resources. In this instance, an LCA was conducted in order to ascertain the environmental impact of the manufacturing process for those cylindrical samples that, according to ASTM E1530:2019, have obtained a higher and lower thermal conductivity (in this case, sample 06 and sample 15 respectively (see Table 10). To compare the environmental impact of the aforementioned samples' manufacturing process to a more conventional manufacturing process, the environmental impact of an additional sample (sample 28) produced by gravity casting followed by machining was evaluated. The LCA for the complete manufacture of samples 06 and 15 included the following two processes: (1) printed by FDM from filaments of PLA-bronze (Cu89/Sn11), and (2) its subsequent debinding and sintering processes considering all 3D printing parameters that were studied. The LCA of the 3D printing process (1) considers the raw materials, energy consumption and PLA emission associated with the manufacturing of all samples 06 and 15.

The PLA emissions were evaluated in terms of the following volatile organic compounds (VOCs), measured in micrograms per hour of FDM printing, as referenced in source [45]: Total Volatile Compunds (TVOC): 199.3 μg/h; Lacitide: 111 μg/h; Acetaldehyd: 18.8 μg/h; 1-Butanol: 17.8 μg/h; Formaldehyd: 7.0 μg/h; Decanal: 4.1 μg/h; Benzaldehyd: 4.1 μg/h; Nonanal: 2.9 μg/h; Caprolactam: 7.4 μg/h; Styrene: 1.6 μg/h and Ethanol: 120 μg/h. The LCA of the debinding and sintering process (2) considers the energy consumption and the complete PLA and activated carbon incineration and, consequently, the emission of several gases. Thus, the CO_2 emissions pertaining to PLA that were taken into account in this study were 2639 g/kg of PLA that was burned [41]. For the activated carbon incineration, the values of emissions considered (in g/kg of activated carbon) were: NO_x (0.14 g/kg); CO (155 g/kg); CO_2 (2567 g/kg) and CH_4 (7.8 g/kg) [42]. Finally, The LCA for the whole manufacture of sample 28 included the following two processes: (3) gravity casting and (4) machining from remains of sample of bronze Cu89/Sn11. The LCA of the gravity casting process (3) considers the energy consumption and the addition of 40 g of sodium tetraborate. The addition of 1 g of sodium tetraborate at high temperature generates approximately 0.208 g of carbon dioxide (CO_2). This product is used in bronze casting as a fluxing agent, facilitating the fusion of metals and eliminating impurities, generating 24.9 g of sodium metaborate $NaBO_2$ that acts as an oxidation protector [46]. Finally, the LCA of the machining process (4) considers the energy consumption, the bronze shavings generated (49.08 g), as well as the addition of 10 g of cutting fluids and coolants. Finally, Table 5 provides a comprehensive summary of the electrical power consumption associated with the production of all the samples studied, as determined by their respective manufacturing processes. These power measurements were obtained using a D52-2047 power meter. The table shows that the electrical power consumption for printing samples using a 0.6 nozzle (sample 15) is lower compared to the electrical power consumption for samples utilizing a 1.0 mm nozzle (sample 06). The data that is shown makes sense, as reducing the diameter of the nozzle leads to an increase in friction losses. This leads to an increase in the electrical power required for printing. The table also shows that, as the sintering temperature rises, the electrical powers required in this process also rises (sample 06 with a sinterizing temperature of 845 °C while sample 15 with 865 °C). Finally, it also seen that the processes that demand the most electrical power are gravity casting and machining.

In the current work, the scope of the LCA was gate-to-gate, and was dedicated exclusively to the manufacturing processes inside the laboratory (3D printing by FDM + sinterizing; and gravity casting + machining). The functional unit that was considered in this investigation was matched to the mass of each sample studied prepared for thermal conductivity in accordance with ASTM E1530:2019 dimensions. The environmental inventory was compiled using inputs from the Ecoinvent 3 database. Table 6 shows the data required to establish the environmental inventory for manufacturing the bronze Cu89/Sn11 samples in accordance with the ASTM E1530:2019 by 3D printing, debinding and sintering. Similarly, Table 7 shows the data required for the environmental inventory by gravity casting and machining process.

Table 5
Electrical power required for the production of samples 06, 15 and 18, according to its manufacturing process.

Manufacturing process	Sample 06	Sample 15	Sample 28
FDM 3D printing [kWh]	0.08	0.15	–
Debinding and sintering [kWh]	4.33	4.43	–
Gravity casting [kWh]	–	–	6.5
Machinning [kWh]	–	–	0.3

Table 6
Data required to establish the environmental inventory for manufacturing the bronze Cu89/Sn11 samples 06 and 15 by 3D FDM printing, debinding and sintering in accordance with the ASTM E1530:2019.

Energy/Material	Item description in Simapro® v.9.2.0.2. software
• Electricity [kwh]: consumed by FDM 3D printing.	• Electricity, (Europe without Swizerland) low voltage
• Electricity [kwh]: consumed by debinding and sintering.	• Electricity, (Europe without Swizerland) low voltage
• Polylactide [g]: Material for FDM 3D printing.	• Polylactide, granulate {GLO} market
• Bronze Cu89/Sn11 [g]: Material for FDM 3D printing.	• Bronze {GLO} market
• Activated carbon [g]: Material for sintering.	• Activated carbon, granular {GLO} market
Emissions into the atmosphere	**Item description in Simapro® v.9.2.0.2. software**
• CO_2 [g]: gas emision from carbon activated incineration.	• Carbon dioxide
• CO [g]: gas emision in carbon activated incineration.	• Carbon monoxide
• CH_4 [g]: gas emision in carbon activated incineration.	• Methane
• NOx [g]: gas emision in carbon activated incineration.	• Nitrogen oxides
• TVOC [g]: volatile organic compouds emision by FDM.	• VOC, volatile organic compouds.
• Lacitide [g]: volatile emision by FDM.	• Lactic acid
• Acetaldehyd [g]: volatile emision by FDM.	• Acetaldehyde
• 1-butanol [g]: volatile emision by FDM.	• 1-butanol
• Formaldehyd [g]: volatile emision FDM.	• Formaldehyde
• Decanal [g]: volatile emision FDM.	• 1- Decanol
• Benzaldehyb [g]: volatile emision FDM.	• Benzaldehyde
• Nonanal [g]: volatile emision FDM.	• 1- Nonanol
• Caprolactam [g]: volatile emision FDM.	• Caprolactam
• Styrene [g]: volatile emision FDM.	• Styrene
• Ethanol [g]: volatile emision FDM.	• Ethanol

Table 7
Data required to establish the environmental inventory for manufacturing the bronze Cu89/Sn11 sample 28 by gravity casting and machining process in accordance with the ASTM E1530:2019.

Energy/Material	Item description in Simapro® v.9.2.0.2. software
• Electricity [kwh]: consumed by gravity casting.	• Electricity, (Europe without Swizerland) low voltage.
• Electricity [kwh]: consumed by machining.	• Electricity, (Europe without Swizerland) low voltage.
• Bronze Cu89/Sn11 [g]: Material for gravity casting.	• Bronze {GLO} market.
• Sodium tetraborate [g]: Material for gravity casting.	• Boric acid, anhydrous, powder {GLO} market.
• Cutting and coolant fluids use in machining [g].	• Lubricating oil {RER} market for lubricating oil Cut-off,S.
• CO_2 [g]: gas emision in sodium tetraborate reaction.	• Carbon dioxide.
• Bronze Cu89/Sn11 [g]: bronze machining shavings	• Scrap bronze {Europe without Switzerland} APOS, S.
• Sodium metaborate (NaBO2) [g]: prevents oxidation of bronze's fusion.	• 2,4-D sodium salt.

3. Results and discussion

3.1. Determination of mass and volumen reduction percentage

As mentioned above, after the debinding and sintering processes, the green samples suffer thermal shrinkage in the X, Y, and Z axes, which is very difficult to predict. To determine precisely each of the shrinkages,

Table 8
Masses of green and sintered PLA-bronze hexahedron samples and their X, Y, and Z thermal shrinkages in %.

Hexaedrom Samples	Gr. Mass [g]	*Sint. Mass [g]*	%X	%Y	%Z	Sample	Gr. Mass [g]	*Sint. Mass [g]*	%X	%Y	%Z
01	*10.40*	*9.55*	*5.3*	*5.3*	*5.8*	*15*	*10.35*	*9.25*	*8.6*	*8.6*	*9.0*
02	*10.36*	*9.25*	*8.3*	*8.3*	*8.5*	*16*	*10.96*	*9.65*	*13.8*	*13.7*	*14.2*
03	*10.52*	*9.41*	*10.4*	*10.2*	*10.8*	*17*	*10.88*	*9.55*	*14.1*	*14.1*	*14.3*
04	*10.38*	*9.42*	*7.3*	*7.1*	*7.7*	*18*	*10.36*	*9.27*	*7.5*	*7.6*	*7.8*
05	*10.55*	*9.43*	*9.3*	*9.1*	*9.7*	*19*	*10.41*	*9.56*	*6.4*	*6.3*	*6.6*
06	*10.96*	*9.67*	*13.1*	*13.0*	*13.4*	*20*	*10.48*	*9.27*	*11.0*	*11.0*	*11.5*
07	*10.76*	*9.41*	*14.9*	*15.0*	*15.5*	*21*	*10.89*	*9.55*	*14.1*	*14.2*	*14.6*
08	*10.96*	*9.63*	*14.2*	*14.3*	*14.8*	*22*	*10.48*	*9.27*	*10.6*	*10.7*	*11.1*
09	*10.73*	*9.43*	*13.6*	*13.8*	*14.1*	*23*	*10.54*	*9.50*	*9.5*	*9.3*	*9.9*
10	*10.52*	*9.37*	*9.5*	*9.4*	*9.6*	*24*	*10.52*	*9.39*	*9.9*	*10.0*	*10.3*
11	*10.49*	*9.30*	*10.3*	*10.3*	*10.5*	*25*	*10.88*	*9.58*	*13.0*	*13.2*	*13.4*
12	*10.41*	*9.54*	*6.1*	*6.1*	*6.4*	*26*	*10.38*	*9.41*	*7.0*	*7.1*	*7.5*
13	*10.37*	*9.40*	*6.8*	*6.8*	*7.1*	*27*	*10.72*	*9.39*	*14.4*	*14.2*	*14.8*
14	*10.54*	*9.48*	*9.2*	*9.2*	*9.7*	-			-	-	-

27 hexahedrons with dimensions 20 mm × 20 mm × 20 mm were printed in PLA-bronze and subsequently sintered. After the samples were cooled at room temperature, they were extracted from the crucible. Then, their masses and shrinkages in each of their axes were determined. Table 8 shows the masses corresponding to the green and sintered hexahedron samples that were manufactured in PLA-bronze, along with their respective thermal shrinkages in the X, Y and Z axes %. The table shows that PLA-bronze samples experienced a marginally greater degree of shrinkage in the Z-direction than in the X or Y directions. This shrinkage in the Z axis can be attributed to the gravitational effects that manifest themselves during the sintering process [8]. Additionally, the table reveals a correlation between layer height and shrinkage along the Z-axis. This can be attributed to a densification in the samples' sintering stage. For instance, samples 01, 05, and 06 exhibit %Z shrinkage of 5.8 %, 9.7 %, and 13.4 %, respectively, corresponding to nozzle diameters of 0.6 mm, 0.8 mm, and 1.0 mm. However, the table also shows that, as the layer's height increases, the shrinkage in the Z axis also increases. So for example, samples 01, 05, and 06 show %Z shrinkage of 5.8 %, 9.7 %, and 13.4 %, respectively, corresponding to nozzle diameters of 0.6 mm, 0.8 mm, and 1.0 mm. However, the shrinkage values in the X and Y directions were very similar for each of the samples studied. In the table it is also is seen that sample 07 is the one that experienced the greatest shrinkage (nozzle diameter = 1.0; flow rate = 100 % and sintering temperature = 865 °C), whereas sample 01 is the one that experienced the least shrinkage (nozzle diameter = 1.0 mm; flow rate = 110 % and sintering temperature = 845 °C). The results indicate that, as the nozzle diameter, flow rate and sintering temperature increases, the shrinkage also increases.

After the thermal shrinkage in the X, Y, and Z axes were determined, they were considered to model and print the 27 PLA-bronze cylindrical samples in accordance with the standardized ASTM E1530:2019 test. Table 9 provides for both green and sinterized cylindrical samples, the mass, diameter and height values, as well as their mass reduction, their diameter and height thermal shrinkages. The samples were conducted in triplicate to ensure repeatability and minimize discrepancies in the experimental results. The relative deviation was maintained within the order of ±0.04 % for the dimensions of the samples in all axes (X, Y, Z), and within the order of ±0.9 % for the thermal conductivity. The corresponding average results were reported in Tables 9 and 10 respectively. In considering the percentages of thermal shrinkage, the table

Table 9
Masses, diameters, heights and thermal shrinkages for the green and sintered PLA-bronze cylindrical samples.

	Green Samples			Sinterized Samples			Reduction Percentages		
Cilindrical Samples	*Mass [g]*	*Diam. [mm]*	Height [mm]	*Mass [g]*	*Diam. [mm]*	Height [mm]	*%Mass [%]*	*%Diam. [%]*	*%Heigh [%]*
01	*84.07*	*52.8*	*5.8*	*77.18*	*49.9*	*5.5*	*8.19*	*5.4*	*5.7*
02	*82.71*	*54.4*	*6.0*	*73.99*	*49.9*	*5.5*	*10.54*	*8.2*	*8.6*
03	*86.18*	*55.8*	*6.2*	*77.03*	*50.1*	*5.5*	*10.62*	*10.3*	*10.7*
04	*83.23*	*54.0*	*6.0*	*75.45*	*50.1*	*5.5*	*9.36*	*7.2*	*7.6*
05	*87.02*	*55.0*	*6.2*	*77.79*	*50.0*	*5.6*	*10.61*	*9.2*	*9.6*
06	*90.05*	*57.4*	*6.5*	*79.44*	*49.9*	*5.6*	*11.78*	*13.0*	*13.3*
07	*88.21*	*58.7*	*6.4*	*77.07*	*49.9*	*5.4*	*12.62*	*15.0*	*15.4*
08	*90.12*	*58.3*	*6.4*	*79.27*	*50.0*	*5.5*	*12.04*	*14.3*	*14.7*
09	*88.19*	*58.0*	*6.3*	*77.59*	*50.0*	*5.4*	*12.02*	*13.7*	*14.0*
10	*86.16*	*55.2*	*6.2*	*76.76*	*50.1*	*5.6*	*10.91*	*9.4*	*9.7*
11	*85.43*	*55.6*	*6.0*	*75.85*	*49.9*	*5.4*	*11.21*	*10.2*	*10.6*
12	*84.13*	*53.3*	*5.8*	*77.08*	*50.0*	*5.4*	*8.38*	*6.0*	*6.4*
13	*83.12*	*53.5*	*6.0*	*75.46*	*49.9*	*5.6*	*9.22*	*6.7*	*7.0*
14	*86.95*	*55.2*	*6.1*	*78.11*	*50.0*	*5.5*	*10.17*	*9.3*	*9.7*
15	*82.69*	*54.8*	*6.1*	*73.85*	*50.0*	*5.5*	*10.69*	*8.7*	*9.1*
16	*89.86*	*57.9*	*6.5*	*79.12*	*50.0*	*5.6*	*11.95*	*13.7*	*14.1*
17	*89.17*	*58.2*	*6.5*	*78.37*	*50.1*	*5.6*	*12.12*	*14.0*	*14.3*
18	*82.72*	*54.1*	*6.0*	*74.25*	*50.1*	*5.5*	*10.24*	*7.5*	*7.8*
19	*83.98*	*53.3*	*6.0*	*77.10*	*50.1*	*5.6*	*8.19*	*6..3*	*6.6*
20	*85.41*	*56.3*	*6.1*	*75.49*	*50.1*	*5.4*	*11.62*	*11.1*	*11.4*
21	*89.20*	*58.3*	*6.4*	*78.29*	*50.1*	*5.5*	*12.23*	*14.2*	*14.6*
22	*85.42*	*56.0*	*6.3*	*75.61*	*50.0*	*5.6*	*11.48*	*10.7*	*11.1*
23	*87.13*	*55.2*	*6.0*	*78.47*	*50.0*	*5.4*	*9.94*	*9.4*	*9.8*
24	*86.22*	*55.6*	*6.2*	*76.98*	*50.1*	*5.6*	*10.72*	*10.0*	*10.4*
25	*89.21*	*57.5*	*6.4*	*78.59*	*50.0*	*5.5*	*11.90*	*13.1*	*13.4*
26	*83.30*	*53.9*	*6.0*	*75.54*	*50.1*	*5.6*	*9.31*	*7.1*	*7.4*
27	*88.21*	*58.3*	*6.6*	*77.26*	*50.0*	*5.6*	*12.42*	*14.3*	*14.7*

Table 10
Density and thermal conductivity values obtained.

Sample	*Density [g/cm³]*	*Thermal Conductivity [W/m·K]*	Sample	*Density [g/cm³]*	*Thermal Conductivity [W/m·K]*
01	*7.30*	*84.75*	*15*	*6.97*	*83.45*
02	*7.01*	*83.77*	*16*	*7.47*	*87.25*
03	*7.24*	*85.46*	*17*	*7.38*	*86.32*
04	*7.09*	*84.22*	*18*	*6.98*	*83.93*
05	*7.35*	*86.53*	*19*	*7.25*	*84.51*
06	*7.52*	*87.61*	*20*	*7.11*	*84.35*
07	*7.29*	*84.11*	*21*	*7.37*	*85.03*
08	*7.48*	*87.13*	*22*	*7.14*	*85.12*
09	*7.32*	*85.83*	*23*	*7.40*	*86.54*
10	*7.22*	*85.91*	*24*	*7.23*	*85.64*
11	*7.17*	*85.64*	*25*	*7.42*	*86.24*
12	*7.27*	*84.62*	*26*	*7.10*	*84.38*
13	*7.14*	*84.48*	*27*	*7.30*	*85.86*
14	*7.36*	*86.35*	*28*	*8.88*	*116.0*

reveals that the measured values of the diameter and height of each sintered cylindrical sample closely align with the required dimensions (50 mm for diameter and 5.5 mm for height). Additionally, the table shows that samples 07 and 01 exhibit, respectively, the greatest and least mass reduction percentages, as well as the greatest and smallest diameter and height thermal shrinkages. These results show that the effects of thermal shrinkage on hexahedrons and cylindricals are fairly similar. To date, no comprehensive research has been carried out on the mechanical and thermal properties of parts manufactured by FDM and sintered subsequently using PLA (Cu89/Sn11) bronze filament with a bronze fraction over 87 wt%. However, there are studies in which these properties have been determined for the PLA-copper filament [7]. The results obtained in the current work show that the minimum of mass reduction obtained was 8.19 %, and it is achieved for the sample 01 (nozzle diameter = 1.0; flow rate = 100 % and sintering temperature = 845 °C). With these same printing parameters, similar results were achieved for PLA-copper samples (copper fraction over 90 wt%), which is the mass reduction obtained for this material of 8 % [5]. For the shrinkage values acquired, Table 9 shows that the reduction in diameter fluctuates between 5.7 % and 15.4 %, whereas the reduction in heights (Z-axis) ranges from 5.4 % to 15 %. Similar results were obtained for PLA-copper samples, with a copper fraction over 95 wt% [8]. In this work, the samples PLA-copper exhibited shrinkages of 13.2 %, 13.4 % and 13.8 % along the X, Y and Z axes, respectively. Additional research has shown that PLA-bronze samples (Cu90/Sn10) with a bronze percentage above 87.4 wt% exhibit shrinkage values of 2.4 %, 27.1 %, and 19 % in the X, Y, and Z axes, respectively [28]. The printing parameters considered in the referenced study were as follows: nozzle diameter of 0.6 mm, layer height of 0.1 mm, print speed of 20 mm/s, flow rate of 130 % and sintering temperature = 870 °C. These values correspond to the findings of the current work, which indicate that an increase in flow rate and sintering temperature results in a corresponding increase in shrinkage.

Finally, Table 10 shows the density and thermal conductivity values for each of the 27 sintered PLA-bronze cylindrical samples. The densities were established using the Archimedes method specified in ASTM B962 [47], whereas the thermal conductivity, as mentioned above, were determined following the guidelines of ASTM E1530:2019. Also, the last row of the table includes the density and thermal conductivity for sample 28 (manufactured by gravity casting and machining).

For the first 27 samples manufactured by FDM, the density values range from 6.97 g/cm^3 to 7.52 g/cm^3, corresponding to samples 15 and 06, respectively, as can be observed in the table. Analogous values were documented in Ref. [28], wherein the sintered PLA-bronze samples had a density value of 7.4 g/cm^3. Also, the aforementioned samples had the maximum and minimum thermal conductivity values, that is, 87.61 W/m·K and 83.45 W/m·K for samples 06 and 15 respectively. The observed correlation between density and thermal conductivity indicates that an increase in density corresponds to a rise in the thermal conductivity of the sintered material [7]. In the preliminary investigation conducted by Lostado et al. [9], similar values of thermal conductivity were observed for the identical material. The average value obtained, as previously stated, was 82.68 W/m·K. The research considered the following printing parameters: nozzle diameter of 0.6 mm, layer height of 0.3 mm, print speed of 30 mm/s, flow rate of 100 % and sintering temperature of 858 °C. Finally, the density and thermal conductivity corresponding to sample 28 manufactured by gravity casting and machining were, respectively, 8.88 g/cm^3 and 116 W/m·K, which are very close to those of pure bronze (Cu89/Sn11). Previous research results suggest that thermal conductivity is mainly influenced by the powder material, its proportion with the polymer, and the debinding and sintering processes. For example, other researchers mentioned above, such as Ebrahimi and Ju [7], obtained for a polymer-copper composite (with a copper powder fraction between 87.0 % and 90.7 %) thermal conductivity values. These are somewhat lower than those obtained in the current research (30 W/m·K and 60 W/m·K). The lower and higher thermal conductivity values obtained corresponded to sintering temperatures of 980 °C for 50 min and 1080 °C for 10 min. Other authors such as Cañadilla et al. [8] determined the thermal conductivity of samples that were manufactured with polymer-copper composite filament with over 95 wt% copper powder fraction using FDM. After the sintering process, the conductivity values that were obtained were 363 ± 9 W/m·K.

Fig. 6 illustrates the relationship between thermal conductivity and density with respect to nozzle diameter and flow rate % at temperatures of 845, 855, and 865 °C. Fig. 6a, b and c show the variations in thermal conductivity at temperatures of 845, 855, and 865 °C, respectively. Meanwhile, Fig. 6d, e and f show the variations in density at the same temperatures. It can be generally gathered from the data that the thermal conductivity of the samples increases in line with their density. Conversely, an examination of Fig. 6c reveals that, when the diameter of the nozzle is 1.0 mm and the flow rate values are 105 % and 110 %, the thermal conductivity values decline as the density of the samples rises.

Additionally, a statistical analysis of the data was carried out with the SPSS software [48] in order to determine which printing parameters were the most affected density and thermal conductivity. First, a Kolmogorov-Smirnov test using the Lilliefors significance correction was applied to the data collected in Tables 4 and 10. The results of the test confirm that the data follows a normal distribution. In addition, a Levene test performed confirmed the homogeneity of variances. Finally, an analysis of variance (ANOVA) computes P-values <0.05 for the printing parameters Nozzle Diameter and for Flow Rate on the variables density and thermal conductivity. It indicates a statistically significant result. On the contrary, P-values of 0.944 and 0.44 are associated for the sintering temperature on these same variables respectively. The latter would indicate that sintering temperature, in this case between 845°c and 865 °C, would barely affect the density and thermal conductivity. The results in Table 10, as well as the statistical analysis, suggest that smaller nozzle diameters and reduced infill lead to lower values for both density and thermal conductivity. In order to identify the reason for the significant variation in thermal conductivity seen among the sintered PLA bronze samples, a microstructure analysis and chemical characterization are conducted in Subsection 3.4.

3.2. Environmental impact analysis

Environmental impacts' endpoints were determined by Simapro® v.9.2.0.2. software considering the ReCiPe Endpoint (E) impact methodology. In this case, the impact on human health, ecosystems and resources environmental impacts endpoint's associated with the production of bronze Cu89/Sn11 samples in accordance with the ASTM E1530:2019 are detailed in Table 11. Ecosystems includes climate change, eutrophication, toxicity, photochemical, ozone formation,

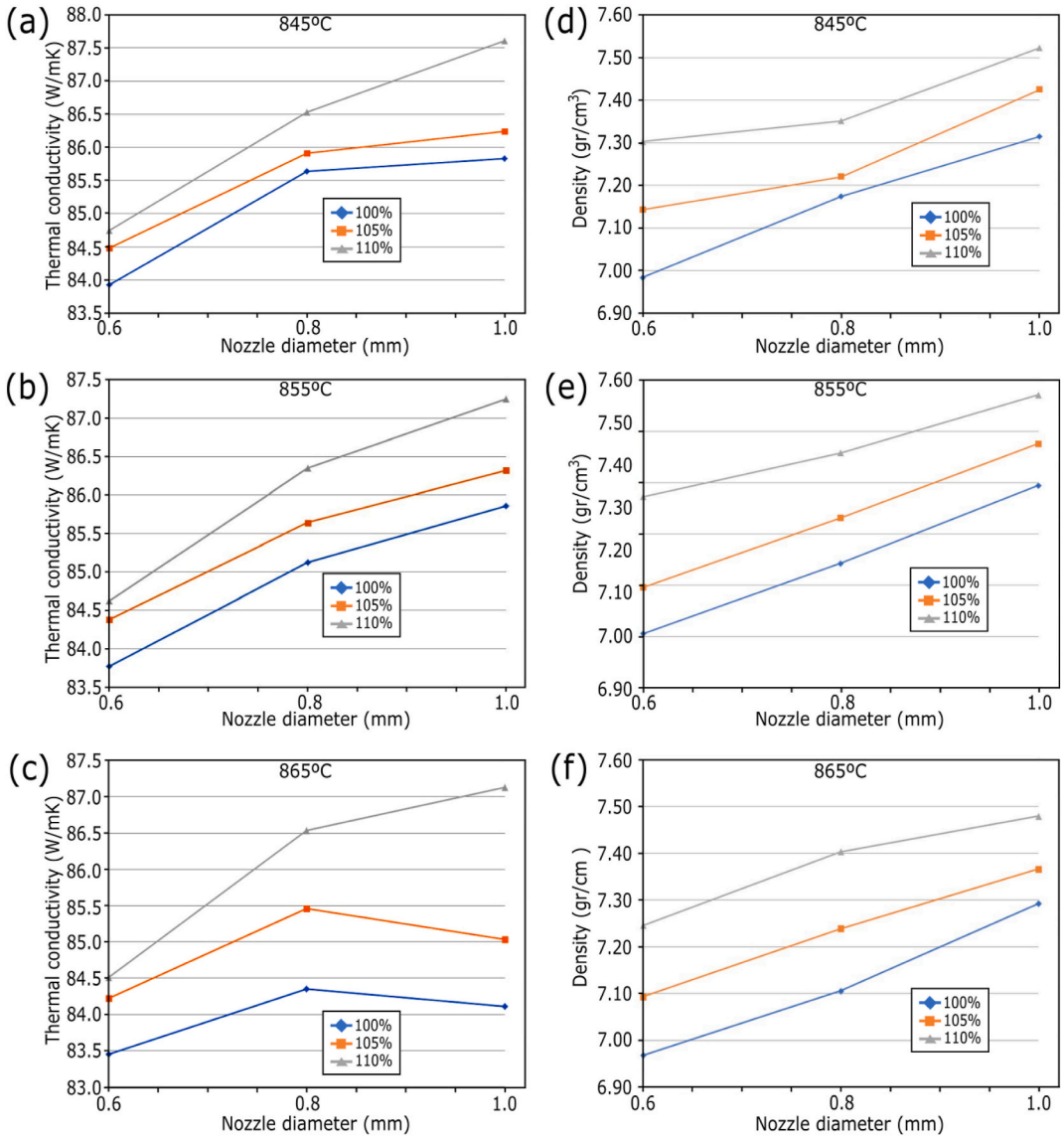

Fig. 6. Variations in thermal conductivity vs. nozzle diameter: (a) at 845 °C. (b) at 855. (c) at 865 °C; Variations in density vs. nozzle diameter: (d) at 845 °C. (e) at 855 °C. (f) at 865 °C.

Table 11
Environmental impact of manufacturing Cu89/Sn11 samples 06, 15 and 28 in accordance with the ASTM E1530:2019, calculated as ReCiPe 2016 Endpoint (E) v1.04.

Impact category	Units	Sample 06: FDM, debinding and sintering	Sample 15: FDM, debinding and sintering	Gravitiy casting and machinning
Human healt	DALY	0.0030078963	0.0028207683	0.0054790072
Ecosystems	species.yr	1.7647595E-6	1.6567042E-6	3.3202805E-6
Resources	USD2013	0.22715895	0.22463355	0.34935046
Human healt (norm.)	Pt	0.033688439	0.031592605	0.06136488
Ecosystems (norm.)	Pt	0.0020930047	0.0019648512	0.0039378526
Resources (norm.)	Pt	8.1095744E-6	8.0194178E-6	1.2471811E-5

acidification, toxicity, land and water use midpoint indicators. Human health includes climate change, ozone depletion, ionizing radiation, fine particulate, matter formation, ozone formation, photochemical, cancer toxicity, non-cancer toxicity and water use midpoints indicators. Finally, resources includes minerals and fossil fuel midpoints indicators [49]. The samples studied in this case were: sample 06 (maximum density and thermal conductivity), sample 15 (minimum density and thermal conductivity) and sample 28 manufactured by gravity casting and machining. The table includes the non-normalized environmental impacts, that are expressed in disability-adjusted life years (DALY); species x years (species.yr) and dollars (USD2013). It also includes the normalized impacts, which are measured in points (pt). When analyzing the unnormalized data, it ca be seen that the most significant impact in this context is related to the resources that are associated with sample 28 manufactured by gravity casting and machining (0.34935046 USD). In contrast, this impact is practically the same for sample 6 and sample 15, with values of 0.22715895 USD and 0.22463355 USD respectively. This impact is directly related to the consumption of energy and raw materials [50], and is notably lower for samples 6 and 15. These last-mentioned two samples have lower consumption of both energy and raw materials when manufactured using FDM followed by debinding

and sintering processes. When analyzing the normalized data, it is clear that the greatest environmental impact is associated with human health for all samples. This is especially significant for the sample manufactured by gravity casting and machining, with a maximum value of 0.06136488 Pt. These data also indicates that, although the number of potentially toxic elements emitted into the atmosphere by samples 6 and 15 is considerably higher than those emitted by sample 8 (see Tables 6 and 7). The greater environmental impacts that are associated with human health correspond to sample 8. This may be due to a greater consumption of electrical power, raw materials and products associated with the bronze fusion and machining process, such as sodium tetraborate and cutting and coolant fluid [18]. When comparing samples 6 and 15 manufactured by the processes of FDM, debinding, and sintering, it is evident that sample 15 exhibits the highest environment impacts. This might be attributed to the fact that the manufacture of this particular sample requires less consumption of electrical power and raw materials than the is needed to manufacture sample 6.

3.3. SEM-EDX analysis

To ascertain the cause of the significant difference in thermal conductivity observed in the PLA-bronze sinterized samples, a microstructure analysis and chemical characterization were both conducted for the sintered samples with the highest and lowest thermal conductivity (sample 06 and 15). A Scanning Electron Microscope (SEM) S-2400 produced by Hitachi Co., Ltd Japan, which worked with an operating voltage of 18 kV, and a Quantax 200 Energy Dispersive X-ray Spectrometer (EDX), produced by Bruker Co., Ltd Germany, were used in this case. Fig. 7a and b shows, respectively, the SEM images of the sample sintered with the highest thermal conductivity obtained (sample 06) at magnifications of 80X and 300X. Similarly, SEM images of the sample sintered with the lowest thermal conductivity obtained (sample 15) also at 80X and 300× magnifications are shown in Fig. 7c and d respectively. In Fig. 7a it is seen that the sintered PLA-bronze has a pore size of about 250 μm in the areas where there is no continuity of particles, whereas that observed in Fig. 7c it is around 500 μm. Furthermore, there is two figures have a notable difference in the shape that the sintered PLA-bronze particles have acquired. Although in Fig. 7b, the particles have a fairly irregular shape with a very rough surface that, has a certain continuity between said particles, the particles in Fig. 7d have a well-defined spherical shape with a smooth surface, but without continuity between them. These spherical particles had a diameter between 10 and 30 μm. Similar results were obtained by Lu et al. [51] for the same PLA-bronze sintered at 832 °C. In that work, spherical particles of bronze powder with diameters between 10 and 50 μm were obtained (similar to those in Fig. 7d). Other researchers, such as Ayeni [52], obtained similar results for this same material. In this case, the sintering temperature was 831 °C and the diameter of the particles obtained was approximately 25 μm.

Also, Fig. 8(a) and (b) show the EDX mapping for the sintered PLA-bronze particles and the rest of the binder that may remain without evaporating that corresponds to the sintered samples with the highest and lowest thermal conductivity respectively. In Fig. 8a, irregularly shaped particles that consist of copper (Cu) and tin (Sn) with traces of oxygen (O) surrounding them are observed. Similarly, Fig. 8b are shown spherical shape particles that consist of copper (Cu) and tin (Sn) with traces of oxygen (O) surrounding these particles. It is noteworthy that, for both figures, these oxygen traces actually correspond to CuO, formed by the oxidation of copper at elevated temperatures [50]. In both figures, traces of carbon (C) and selenium (SE) are barely noticeable. This suggests that the blinder (PLA) completely evaporated during the debinding process.

Also, Table 12 shows the significant elements obtained in Fig. 8(a) and (b) respectively. The table clearly shows that the sample that exhibits the highest thermal conductivity has a greater percentage (wt.%) of Cu (81.91 %) and Sn (10.09 %). Notably, these values closely align with the composition of the manufacturer-provided filament (Cu89/Sn11). This means that the PLA polymer binder has been practically eliminated in this sample. In contrast, the sample with the lowest thermal conductivity contains a lower percentage by weight % (wt.%) of Cu (62.05 %) and Sn (10.06 %), with other elements present such as C (13.92 %), Se (0.57 %) and S(0.14 %). These elements are typical residues from an incineration process of PLA bottom ashes that have not been completely evaporated and are present as traces between the particles of sintered material.

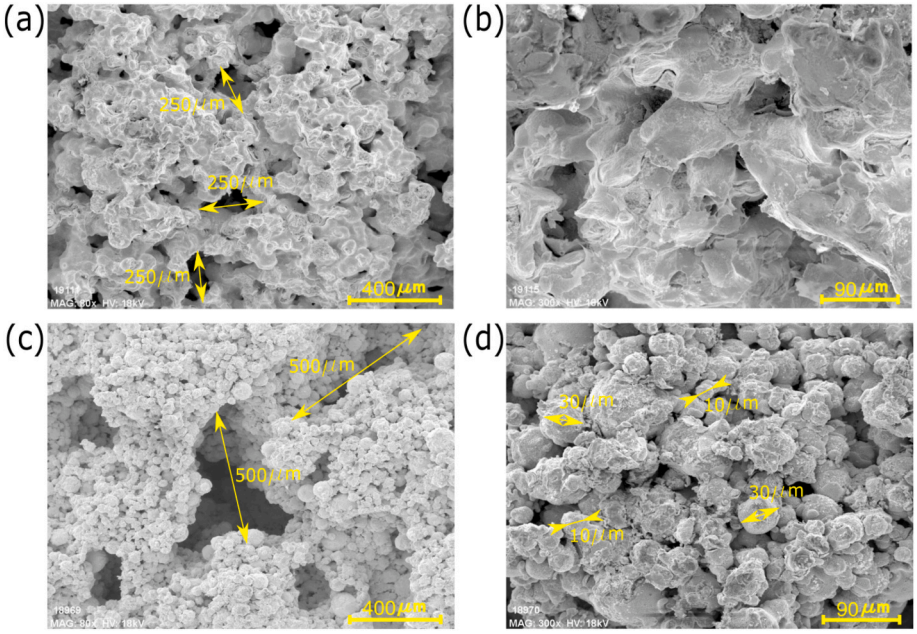

Fig. 7. SEM image of: (a) Sample 06 with the highest thermal conductivity obtained at a magnification of 80×. (b) Sample 06 with the highest thermal conductivity obtained at a magnification of 300×. (c) Sample 15 with the lowest thermal conductivity obtained at a magnification of 80×. (d) Sample 15 with the lowest thermal conductivity obtained at a magnification of 300×.

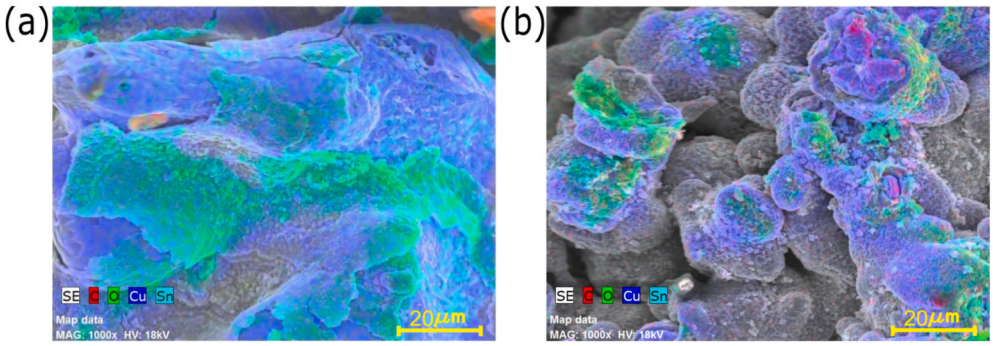

Fig. 8. EDX mapping for the: (a) Sample 06 with the highest thermal conductivity obtained at a magnification of 1000×. (b) Sample 15 with the lowest thermal conductivity obtained at a magnification of 1000×.

Table 12
Results of the EDX analysis in Fig. 8.

Sample 06		Sample 15	
Elements	***Weigth(%)***	Elements	***Weigth(%)***
Cooper (Cu)	81.91 %	***Cooper (Cu)***	62.05 %
Tin (Sn)	10.09 %	***Tin (Sn)***	10.06 %
Carbon (C)	2.11 %	***Carbon (C)***	13.92 %
Oxigen (O)	5.89 %	***Oxigen (O)***	12.85 %
-	–	***Selenium (Se)***	0.57 %
-	–	***Phosphorus (P)***	0.41 %
-	–	***Sulfur (S)***	0.14 %

4. Conclusions

This study sought to explore the feasibility of producing sintered bronze (Cu89/Sn11) by low-cost 3D printing Fused Deposition Modeling (FDM) technology and thermal post-treatment processes. The emphasis was on determining optimal printing parameters and sintering temperature to maximize thermal conductivity while minimizing energy consumption and environmental impact. The sample with a 1.0 mm nozzle diameter, 110 % flow rate, and sintering at 845 °C showed the highest density and thermal conductivity among all samples analyzed: 7.52 g/cm^3 and 87.61 W/m·K, respectively. Conversely, the sample with a 0.6 mm nozzle diameter, 110 % flow rate, and sintering at 865 °C had the lowest values: 6.97 g/cm^3 for density and 83.45 W/m·K for thermal conductivity. Decreasing the nozzle diameter and infill size resulted in lower density and thermal conductivity. Comparatively, a sample manufactured by gravity casting and machining exhibited higher values: 8.88 g/cm^3 for density and 116 W/m·K for thermal conductivity. The SEM image at 80X magnification shows pores of 250 μm in the sample with the highest density and thermal conductivity, whereas the sample with the lowest values has larger pores, around 500 μm. At 300X magnification, the SEM image reveals particle continuity in the high-density sample, whereas the low-density sample displays distinct spherical particles ranging from 10 to 30 μm in size. Finally, the chemical composition of both samples was analyzed to identify significant elements. The sample with the highest thermal conductivity contains a higher weight percentage of Cu (81.91 %) and Sn (10.09 %), whereas the sample with the lowest thermal conductivity has a lower weight percentage of Cu (62.05 %) and Sn (10.06 %). Additionally, the latter sample contains other elements, such as C (13.92 %), Se (0.57 %), and S (0.14 %), typical waste products from a PLA incineration process. These elements remain as traces within the sintered material, affecting its density and thermal conductivity. The results suggest that, with a smaller nozzle size and reduced flow rate, residues from PLA incineration cannot be effectively eliminated during the sintering process, thus impacting the quality of the sintered bronze.

The results of the life cycle assessment (LCA) reveal that the most substantial impact, that is closely tied to energy and raw material consumption (resources), is associated with the sample manufactured by gravity casting and machining (0.34935046 USD). This impact is nearly the same for samples exhibiting the highest and lowest density and thermal conductivities, with values of 0.22715895 USD and 0.22463355 USD, respectively. Normalized data show a significant environmental impact on human health, particularly with the sample manufactured by gravity casting and machining. Although the samples with the highest and lowest density and thermal conductivities emit more potentially toxic elements, the gravity casting and machining process has a greater impact on human health. This is likely due to increased consumption of electrical power, raw materials, and products, such as sodium tetraborate and cutting coolant fluid during bronze fusion and machining.

For future research, it is suggested that the study be expanded by incorporating additional printing parameters, such as shell thickness, printing speed, or infill pattern. Moreover, broadening the investigation by extending the range of sintering temperatures could yield higher density and thermal conductivity values. Additionally, further research is suggested to expand the scope of the current research from “gate-to-gate” to “cradle to gate” or even “cradle to grave” for future works. This would give greater scope to the research since the environmental impacts generated by manufacturing the filaments of PLA-bronze (Cu89/Sn11) that were used in this study could also be included.

CRediT authorship contribution statement

Rubén Lostado-Lorza: Writing – review & editing, Writing – original draft, Validation, Supervision, Software, Methodology, Investigation, Formal analysis, Conceptualization. **Marina Corral-Bobadilla:** Writing – review & editing, Validation, Supervision, Methodology, Formal analysis, Conceptualization. **Celia Sabando-Fraile:** Writing – review & editing, Validation, Methodology, Conceptualization. **Fátima Somovilla-Gómez:** Writing – review & editing, Validation, Methodology.

Declaration of competing interest

The authors declare that they have no known competing financial interests or personal relationships that could have appeared to influence the work reported in this paper.

Data availability

No data was used for the research described in the article.

References

[1] Piping R. Heat transfer components: ASME code for pressure pipping, B31 and American National Standard. 2001.
[2] Klocke F, Kuchle A. Manufacturing processes, vol. 2. Berlin: Springer; 2009. p. 433.

[3] Ramazani H, Kami A. Metal FDM, a new extrusion-based additive manufacturing technology for manufacturing of metallic parts: a review. Prog Addit Manuf 2022;7(4):609–26. https://doi.org/10.1007/s40964-021-00250-x.

[4] https://sintratec.com/how-to-3d-print-metal-parts/.

[5] Cheng CH, Loh CC, Zhang YJ. Simulation of metallic parts by 3D printing using metallic powder–polylactide composite filament. Prog Addit Manuf 2022;7(3):495–508. https://doi.org/10.1007/s40964-022-00287-6.

[6] Roudný P, Syrový T. Thermal conductive composites for FDM 3D printing: a review, opportunities and obstacles, future directions. J Manuf Process 2022;83:667–77. https://doi.org/10.1016/j.jmapro.2022.09.026.

[7] Ebrahimi ND, Ju YS. Thermal conductivity of sintered copper samples prepared using 3D printing-compatible polymer composite filaments. Addit Manuf 2018;24:479–85. https://doi.org/10.1016/j.addma.2018.10.025.

[8] Cañadilla A, Romero A, Rodríguez GP, Caminero MÁ, Dura ÓJ. Mechanical, electrical, and thermal characterization of pure copper parts manufactured via material extrusion additive manufacturing. Materials 2022;15(13):4644. https://doi.org/10.3390/ma15134644.

[9] Lostado-Lorza R, Corral-Bobadilla M, Iñiguez-Macedo S, Somovilla-Gómez F, Sabando-Fraile C. Tensile strength, elastic modulus and thermal conductivity of 3D-Printed components using bronze/PLA filament. 8th Int Conf Smart Sustain Technol SpliT 2023:1–5. https://doi.org/10.23919/SpliTech58164.2023.10193626.

[10] Karwasz A, Osinski F. Literature review on emissions from additive manufacturing by FDM method and their impact on human health. Manag Prod Eng Rev 2020;11(3):65–73. 0.24425/mper.2020.134933.

[11] Landi D, Spreafico C, Russo D. LCA of titanium powder: empirical evidence vs data from patents, possible future applications. Procedia CIRP 2023;116:318–23. https://doi.org/10.1016/j.procir.2023.02.054.

[12] Meshram RB, Haldar N, Sahoo KL. Environmental impacts of brass melting: an Indian case study. Procedia CIRP 2021;98:500–4. https://doi.org/10.1016/j.procir.2021.01.141.

[13] da Silva HG, Ferreira JC, Kelm T, Ivaniski TM. Life cycle assessment of the casting process with the addition of niobium from scrap. SN Appl Sci 2023;5(12):325. https://doi.org/10.1007/s42452-023-05569-4.

[14] Lostado-Lorza R, Corral-Bobadilla M, Íñiguez-Macedo S, Somovilla-Gómez F. Characterization, LCA and FEA for an efficient ecodesign of novel stainless steel woven wire mesh reinforced recycled aluminum alloy matrix composite. J Clean Prod 2023;411:137380. https://doi.org/10.1016/j.jclepro.2023.137380.

[15] Kumar R, Sharma H, Saran C, Tripathy TS, Sangwan KS, Herrmann C. A comparative study on the life cycle assessment of a 3D printed product with PLA, ABS & PETG materials. Procedia CIRP 2022;107:15–20. https://doi.org/10.1016/j.procir.2022.04.003.

[16] Tengzelius J. Life cycle assessment (LCA) of powder metallurgy. Powder Metallurgy World Congress. Kyoto; 2000.

[17] Peng T, Kellens K, Tang R, Chen C, Chen G. Sustainability of additive manufacturing: an overview on its energy demand and environmental impact. Addit Manuf 2018;21:694–704. https://doi.org/10.1016/j.addma.2018.04.022.

[18] Faludi J, Bayley C, Bhogal S, Iribarne M. Comparing environmental impacts of additive manufacturing vs traditional machining via life-cycle assessment. Rapid Prototyp J 2015;21(1):14–33. https://doi.org/10.1108/RPJ-07-2013-0067. 2015.

[19] Standard test method for evaluating the resistance to thermal transmission by the guarded heat flow meter technique. https://www.astm.org/e1530-19.html. [Accessed 9 February 2024].

[20] Bronze filament supplier. Nigrán 2024. https://filament2print.com/es/.

[21] Filament™-TDS Bronze. The virtual foundry, stoughton. 2024. https://thevirtualfoundry.com/.

[22] Liu B, Wang Y, Lin Z, Zhang T. Creating metal parts by fused deposition modeling and sintering. Mater Lett 2020;263:127252. https://doi.org/10.1016/j.matlet.2019.127252.

[23] Yilmaz S, Gul O, Eyri B, Gamze Karsli Yilmaz N, Yilmaz T. Comprehensive characterization of 3D-printed bamboo/poly(lactic acid) bio composites. Polym Eng Sci 2023;63(9):2958–72. https://doi.org/10.1002/pen.2641.

[24] Yilmaz O, Gul B, Eyri, KarsliT NG, Yilmaz. Analyzing the influence of multimaterial 3D printing and postprocessing on mechanical and tribological characteristics. Macromol Mater Eng 2024. https://doi.org/10.1002/mame.202300428.

[25] Agarwala MK, Weeren RV, Bandyopadhyay A, Safari A, Danforth SC, Priedeman WR. Filament feed materials for fused deposition processing of ceramics and metals. In: International solid freeform fabrication symposium; 1996.

[26] Agarwala MK, Weeren RV, Bandyopadhyay A, Whalen PJ, Safari A, Danforth SC. Fused deposition of ceramics and metals: an overview. In: International solid freeform fabrication symposium; 1996.

[27] Galantucci LM, Pellegrini A, Guerra MG, Lavecchia F. 3D printing of parts using metal extrusion: an overview of shaping debinding and sintering technology. In: Proceedings of international scientific conference MMA; 2021. p. 5–12.

[28] Wagner MA, Hadian A, Sebastian T, Clemens F, Schweizer T, Rodriguez-Arbaizar M, Spolenak R. Fused filament fabrication of stainless steel structures-from binder development to sintered properties. Addit Manuf 2022;49:102472. https://doi.org/10.1016/j.addma.2021.102472. 2022.

[29] Dizdar S, Krishna AV. Microstructural and mechanical properties of polylactic acid/tin bronze tensile strength bars additive manufactured by fused deposition modelling. SPS2022. IOS Press; 2022. p. 566–79. https://doi.org/10.3233/ATDE220175.

[30] Fisher RA. Design of experiments. Br Med J 1936;1:554.

[31] Park GJ. Design of experiments. Analytic methods for design practice. 2007. p. 309–91.

[32] Software for desing CAD 3D SOLIDWORKS n.d. https://www.solidworks.com/es/home-page-2021. [Accessed 9 February 2024].

[33] UltiMaker Cura - UltiMaker n.d. https://ultimaker.com/es/software/ultimaker-cura/(accessed February 9, 2024).

[34] Environmental management—life cycle assessment—principles and framework, document ISO 14040 2006. https://www.iso.org/standard/37456.html. [Accessed 9 February 2024].

[35] Environmental management—life cycle assessment—requirements and guidelines, document ISO 14044 2006. https://www.iso.org/standard/38498.html. [Accessed 9 February 2024].

[36] Wach AK. Life cycle assessment (LCA) as the basis for computer-assisted product evaluation. Conf. Mater. 2nd natl. Sci. Technol. Conf. "Ecology Electron. Wars. 2002.

[37] Iswara AP, Farahdiba AU, Nadhifatin EN, Pirade F, Andhikaputra G, Muflihah I, Boedisantoso R. A comparative study of life cycle impact assessment using different software programs. IOP Conf Ser Earth Environ Sci 2020;506:012002. https://doi.org/10.1088/1755-1315/506/1/012002.

[38] Fonseca A, Ramalho E, Gouveia A, Figueiredo F, Nunes J. Life cycle assessment of PLA products: a systematic literature review. Sustainability 2023;15(16):12470. https://doi.org/10.3390/su151612470.

[39] Kokare S, Oliveira JP, Godina R. Life cycle assessment of additive manufacturing processes: a review. J Manuf Syst 2023;68:536–59. https://doi.org/10.1016/j.jmsy.2023.05.007.

[40] Mendes L, Kangas A, Kukko K, Mølgaard B, Säämänen A, Kanerva T, Viitanen AK. Characterization of emissions from a desktop 3D printer. J Ind Ecol 2017;21(S1):S94–106. https://doi.org/10.1111/jiec.12569.

[41] Stabile L, Scungio M, Buonanno G, Arpino F, Ficco G. Airborne particle emission of a commercial 3D printer: the effect of filament material and printing temperature. Indoor Air 2017;27(2):398–408. https://doi.org/10.1111/ina.12310.

[42] Eriksson O, Finnveden G. Plastic waste as a fuel-CO 2-neutral or not? Energy Environ Sci 2009;2(9):907–14. https://doi.org/10.1039/B908135F.

[43] Joshi D, Modi Y. Evaluating environmental impacts of sand cast products using life cycle assessment. 3rd Int. Conf. Res. Des. Eng. Bangalore. 2011:551–8.

[44] Carou D, Lozano JA, León-Mateos F, Sartal A, Gupta MK. An introduction to the use of life cycle assessment in machining. In: Corporate governance for climate transition. Cham: Springer International Publishing; 2023. p. 141–66.

[45] Azimi P, Zhao D, Pouzet C, Crain NE, Stephens B. Emissions of ultrafine particles and volatile organic compounds from commercially available desktop three-dimensional printers with multiple filaments. Environ Sci Technol 2016;50(3):1260–8. https://doi.org/10.1021/acs.est.5b04983.

[46] Wickramasinghe KC, Sasahara H, Abd Rahim E, Perera GIP. Green Metalworking Fluids for sustainable machining applications: a review. J Clean Prod 2020;257:120552. https://doi.org/10.1016/j.jclepro.2020.120552.

[47] ASTM B962. Standard test methods for density of compacted or sintered powder metallurgy (PM) products using Archimedes' principle 2023. https://www.document-center.com/standards/show/ASTM-B962. [Accessed 9 February 2024].

[48] IBM SPSS Statistics n.d. https://www.ibm.com/products/spss-statistics. [Accessed 9 February 2023].

[49] National institute of public health and the environment. Report: ReCiPe 2016 v1.1 A harmonized life cycle impact assessment method at midpoint and endpoint level Report I: Characterization https://www.rivm.nl/en/life-cycle-assessment-lca/recipe.

[50] Yang N, Sheng X, Ti L, Jia H, Ping Q, Li N. Ball-milling transesterification process on biodiesel production: RSM optimization, life cycle assessment and market dynamics analysis. Energy 2023;283:129201. https://doi.org/10.1016/j.energy.2023.129201.

[51] Lu Z, Ayeni OI, Yang X, Park HY, Jung YG, Zhang J. Microstructure and phase analysis of 3D-printed components using bronze metal filament. J Mater Eng Perform 2020;29:1650–6. https://doi.org/10.1007/s11665-020-04697-x.

[52] Ayeni OI. Sintering and characterizations of 3D printed bronze metal filament. Purdue University; 2019.